ADVANCED MATERIALS
www.advmat.de

Biophysically Defined and Cytocompatible Covalently Adaptable Networks as Viscoelastic 3D Cell Culture Systems

*Daniel D. McKinnon, Dylan W. Domaille, Jennifer N. Cha, and Kristi S. Anseth**

Covalently crosslinked synthetic hydrogels are especially suitable as tissue engineering scaffolds due to their well-defined and easily tunable biochemical and biophysical properties. In order to enable complex cell functions like ECM deposition, motility, and spreading, a mechanism for crosslink degradation must be engineered into the material; however, the presence of a degradation trigger can complicate the cellular biophysical microenvironment. Furthermore, covalently crosslinked polymers typically produce a predominantly elastic material, while native tissues are complex viscoelastic structures. Here, we present a step-growth poly(ethylene glycol) (PEG) hydrogel crosslinked by reversible hydrazone bonds. The macromer components are readily synthesized from commercially available precursors, and the resulting gels form rapidly under physiological conditions and provide a non-toxic matrix that is suitable for cell culture. This material is capable of mimicking aspects of the viscoelastic properties of native tissues, and the dynamic stress relaxing crosslinks permit complex cellular functions to occur while retaining the benefits of traditional covalently crosslinked hydrogels. Taken together, these attributes make hydrazone crosslinked hydrogels a unique tool for designing viscoelastic scaffolds and studying cellular responses to scaffold elasticity.

Culturing cells in hydrogels for the purpose of regenerating tissue requires that the polymer matrix accommodate numerous cellular functions, beginning with matrix interactions and morphological changes. This initial adaptation allows encapsulated cells to subsequently engage in an external-internal exchange of information that influences critical processes including proliferation, motility, and extracellular matrix (ECM) deposition.[1–3] To facilitate improved three-dimensional culture environments, early approaches to hydrogel design often incorporated hydrolytically degradable crosslinks, engineered to degrade at a rate that was matched by the rate of the cellular function under study.[4–6] This strategy allowed for uniform ECM elaboration, but in many instances, only local changes in gel properties are desired (e.g., to promote cell spreading), and pre-engineering the degradation rates is often a complex optimization process. Thus, hampered by artificial constraints of bulk property changes at pre-determined rates, researchers developed complementary strategies based on processes that occur in native ECM, where cells bind, degrade and respond to their local proteinaceous microenvironment. For example, Hubbell et al. pioneered the development of hydrogels crosslinked with cell-degradable and integrin binding peptide sequences, which mimicked critical aspects of the biochemical function of ECM.[7,8] Such polymer-peptide gels have permitted researchers to observe and characterize the dynamics of cell spreading,[9–11] migration,[11,12] axon extension,[13,14] proliferation,[15,16] and differentiation in a synthetic three-dimensional matrices.[16,17] However, unlike hydrolytically degradable gels, the cellular microenvironment in cellularly remodeled gels can be dramatically different from that of synthetic and hydrolytically degradable materials, which makes it difficult to characterize and draw conclusions about the role of the local biophysical environment on cell function.

In contrast, a covalently adaptable network responds to cell-induced stress by rapidly breaking and reforming elastically active crosslinks while maintaining stable material properties over time. This allows the material to respond to cell stresses yet provides a uniform scaffold elasticity to enable the elucidation of the effect of biophysical microenvironment on cell function. Given the increasing use of progenitor cells in biomaterials research and the increasing understanding of the role of biomechanical signaling on cell fate,[18–21] such a material should enable the observation of cell behavior in a biophysically defined scaffold. While dynamic bonds have previously been used in biomaterial scaffolds,[22–26] these linkages are supplemented by additional interactions, which precludes the precise and predictable biophysical control of the hydrogel. We sought to use a linkage that was stable enough to maintain the integrity of a crosslinked PEG network for several weeks of cell culture, but that would be labile enough to relax in response to cell-applied stress and allow for cell spreading, process extension, migration, or axon outgrowth to occur. Furthermore, few dynamic chemistries are compatible with cell encapsulation, and previously published covalently adaptable networks have either relied on high temperatures, low pH, or UV light to trigger covalent adaptability.[27–34]

D. D. McKinnon, D. W. Domaille, J. N. Cha, K. S. Anseth
Department of Chemical and Biological Engineering
University of Colorado Boulder
Jennie Smoly Caruthers Biotechnology Building
3415 Colorado Ave, 596 UCB, Boulder, CO, 80303
D. D. McKinnon, K. S. Anseth
BioFrontiers Institute
University of Colorado Boulder
Jennie Smoly Caruthers Biotechnology Building
3415 Colorado Ave, 596 UCB, Boulder, CO, 80303
K. S. Anseth
Howard Hughes Medical Institute University of Colorado Boulder
Jennie Smoly Caruthers Biotechnology Building
3415 Colorado Ave, 596 UCB, Boulder, CO, 80303
E-mail: kristi.anseth@colorado.edu
Tel: 303–735–5336, Fax: 303–492–4341

DOI: 10.1002/adma.201303680

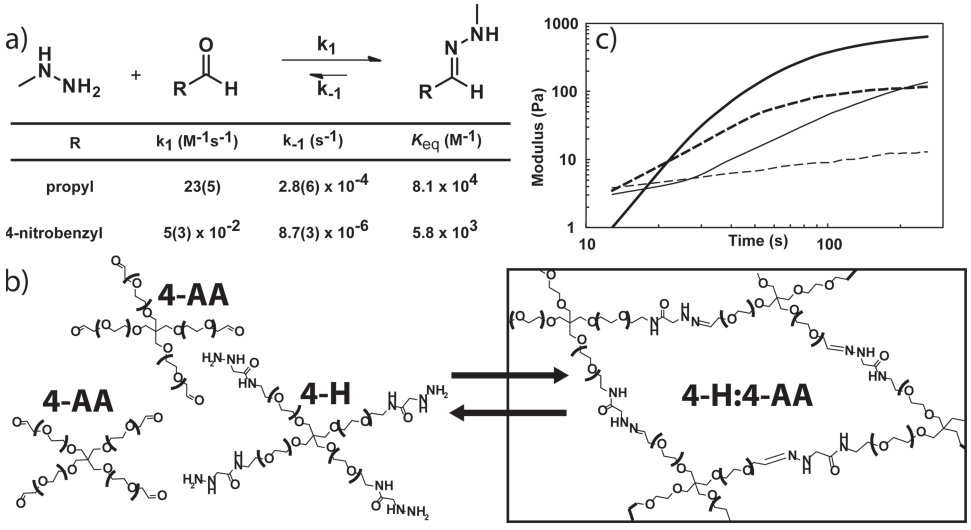

Figure 1. a) Table showing the relevant kinetic and thermodynamic information for reactions between N-methyl hydrazine and butyraldehyde or 4-nitrobenzaldehyde at 25 °C in pH 7.4 buffer containing 1% DMSO. b) Chemical structures of **4-H** and **4-AA** showing reversible gelation. c) Rheological time sweep plot showing rates of gelation. Evolution of 90% of G_∞ occurs in 5 minutes for **4-H:4-AA** (thick solid line, G′; thick dashed line G″) and ca. 1 hour for **4-H:4-BA** (thin solid line, G′; thin dashed line G″).

In order to identify a cytocompatible chemistry that would crosslink hydrogels yet remain dynamic under physiologically relevant conditions, we looked to the field of dynamic covalent chemistry, which is comprised of reversible reactions under thermodynamic control, and include but are not limited to transesterification, acetal exchange, and hydrazone/oxime exchange.[35] We were especially drawn to the hydrazone transimination reaction because it has been used in in vitro biological systems to assemble enzyme substrates[36] and to perform bioconjugations.[37–43] Further, the reaction rate between the hydrazine/alkoxyamine nucleophiles and aldehyde electrophiles and the stability of the resulting hydrazone/oxime are highly dependent on the precise chemical structure of the nucleophilic and electrophilic components; stability half-life values range from minutes to months at pH 7.0, depending on the exact functionality.[39,42] Thus, we hypothesized that a hydrazone crosslinked hydrogel would show covalently adaptable behavior, characterized by a frequency-dependent modulus and stress relaxation, under physiological conditions.

The material presented here is a PEG hydrogel formed through the ligation of an aliphatic hydrazine-terminated multi-arm PEG macromer with either a benzaldehyde- or an aliphatic aldehyde-terminated multi-arm PEG macromer. Gel formation occurs rapidly at physiological pH and temperature. The resulting cytocompatible covalently adaptable hydrogel allows a large degree of tunability of the biochemical and biophysical microenvironment, captures both the modulus and adaptability of native tissue, and enables the encapsulation of a diverse array of cell types. We believe that this material system will provide a unique platform to culture cells in three-dimensions, allow for improved reproduction of the stress relaxation found in native ECM, and permit the determination of how dynamic changes in the local biophysical environment influence cellular functions.

In an effort to identify hydrazine and aldehyde constituents that would react on a timescale compatible with hydrogel formation and cell encapsulation, we first investigated the kinetic and thermodynamic properties of small-molecule hydrazones that result from the reaction of a model aliphatic hydrazine, methylhydrazine, with two model aldehydes: an aliphatic aldehyde, butyraldehyde, and an aryl aldehyde, 4-nitrobenzaldehyde. Hydrazone formation was monitored by UV-vis spectroscopy, and the data were fitted to a bimolecular reversible kinetic model.[38] We assume equimolar starting concentrations of reactants and that the concentration of the hydrazone is simply the initial concentration of one reactant less the current concentration of that reactant. These assumptions simplify the rate equation to Equation (1),

$$\frac{d[A]}{dt} = -k_1[A]^2 + k_{-1}([A]_0 - [A]) \quad (1)$$

where A is the concentration of either one of the reactants. The solution to the equation is derived in Dirksen et al. and allows the calculation of k_1, k_{-1}, and K by monitoring the evolution of the hydrazone bond or the disappearance of one of the reactants.[38] The reaction between methylhydrazine (25 μM) with butyraldehyde (25 μM) was rapid and reached equilibrium in less than an hour in pH 7.4 buffer (Figure Supporting Information, SI 1a). In contrast, the reaction of methylhydrazine (25 μM) and 4-nitrobenzaldehyde (25 μM) took several days to reach equilibrium (Figure SI 1b). The calculated forward rate constants (k_1), back rate constants (k_{-1}), and equilibrium constants (K_{eq}) are summarized in **Figure 1**a.

These data provided convincing evidence that both the aliphatic and aryl hydrazone bonds would form rapidly enough to crosslink a cell-laden hydrogel, as the rate constants for aliphatic and aryl hydrazone formation fall close to the range of

Adv. Mater. 2013,
DOI: 10.1002/adma.201303680

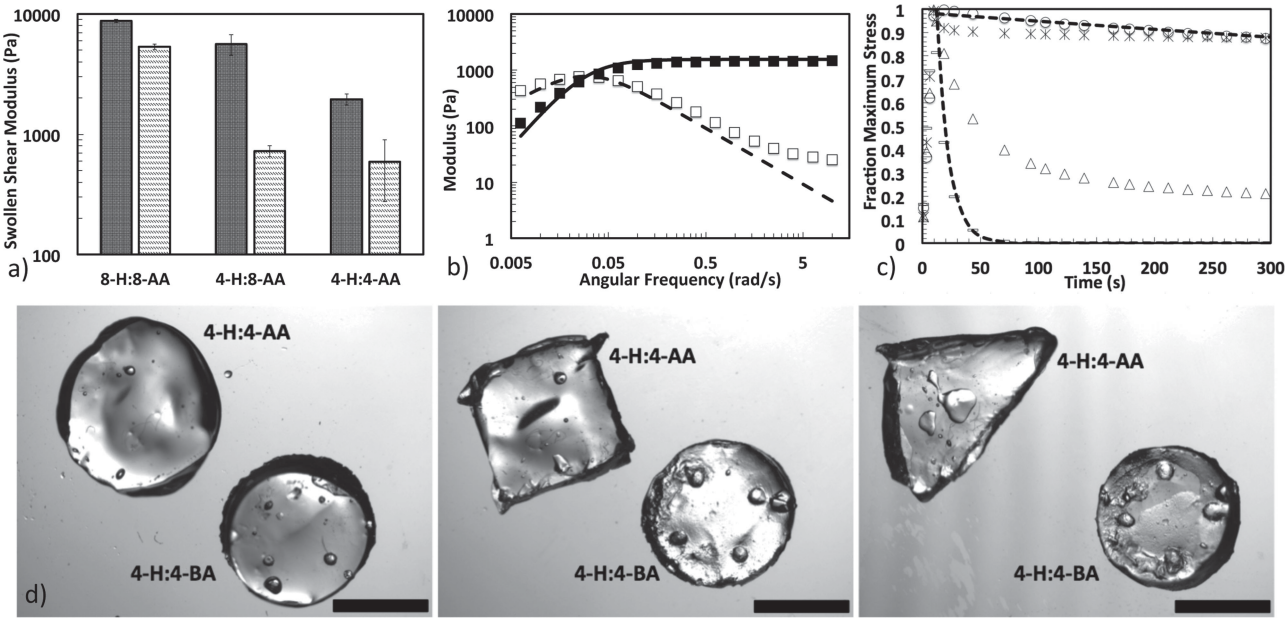

Figure 2. a) Hydrogel modulus can be controlled by incorporating crosslinkers of different functionalities or varying the stoichiometry of functional groups (dark bars, on stoichiometry; light bars 50% excess hydrazine, Student's t-test, $p < 0.05$). b) **4-H:4-AA** shows frequency-dependent crossover below 0.03 rad/s, which indicates that it behaves as a Maxwellian viscoelastic fluid (filled squares, G′; empty squares, G″; solid line, G′ Maxwell fit; dashed line, G″ Maxwell fit).[43] c) Stress relaxation is strongly dependent on the ratio of aliphatic to aryl aldehyde crosslinker, with relaxation times ranging from tens of seconds to tens of hours (bars, 100:0 **4-AA:4-BA**; triangles, 80:20; circles, 0:100). When the mole fraction of **4-BA** crosslinker crosses the percolation threshold of the system, the stress relaxation behavior collapses to that of 0:100. Stress relaxation of **4-H:4-AA** and **4-H:4-BA** are in good agreement with the Maxwell model (dashed lines). Covalent adaptability can be abolished upon treatment by sodium cyanoborohydride, which reduces the hydrazone bond to the corresponding secondary hydrazine (asterisks). d) Stress relaxation can be shown macroscopically through molding. **4-H:4-AA** and **4-H:4-BA** were pressed into square and triangular molds for 60 s, with **4-H:4-AA** adopting the shape of the mold as a viscoelastic fluid and **4-H:4-BA** retaining its shape as a more elastic solid (scale bar = 3 mm).

reported rate constants for other hydrogel crosslinking chemistry, such as those for dibenzylcyclooctyne-azide (2.1 M^{-1} s^{-1}) and vinyl sulfone-thiol couplings (0.17 M^{-1} s^{-1}).[7,44–47] Thus, we functionalized 4-arm 20 kDa and 8-arm 10 kDa PEG macromers with aliphatic hydrazine end groups (**4-H, 8-H)** and 4-arm 10 kDa and 8-arm 10 kDa PEG macromers with either benzaldehyde (**4-BA, 8-BA)** or aliphatic aldehyde (**4-AA, 8-AA)** end groups. Gram-scale quantities of the macromers are synthetically available in 1–2 steps from inexpensive commercially available precursors, which renders this system accessible to a wide range of biomedical, chemical, and polymer engineering labs. Mixing 18 mM (72 mM functional groups) solutions of either **4-H** and **4-AA** (Figure 1b) or **4-H** and **4-BA** resulted in the formation of a hydrogel at room temperature and pH 7.4. The rheological properties of the gels were investigated under shear, and the results are shown in **Figures** 1 and **2**. **4-H:4-AA** reaches its crossover point in tens of seconds. Evolution of 90% of its final elastic modulus is achieved in 5 minutes, which can be predicted by fitting modulus evolution data to Equation (2),

$$G(t) = G_\infty - Ae^{-Bt} \tag{2}$$

where G_∞ is the plateau modulus and A and B are fit parameters. **4-H:4-BA** reaches its final modulus in ca. 1 hour at pH 7.4, but this process is highly pH dependent (Figure 1c, Figure SI 2a).

In addition to exerting control over the stress relaxation characteristics of these materials, we can also control equilibrium modulus by varying the size and functionality of each macromer. Furthermore, because the crosslinking density is linearly related to modulus through Equation (3),

$$G = kTQ^{-1/3}\rho_x \tag{3}$$

where k is Boltzmann constant, T is the temperature, Q is the volume swelling ratio, and ρ_x is the crosslinking density, the final material modulus can be systematically varied to target a tissue or magnitude of interest. In Figure 2a, the swollen shear modulus varied from ~600 Pa (**4-H:4-AA**, 2:1) to ~9 kPa (**8-H:8-AA**), and all of the values are in reasonable agreement with that predicted by rubber elasticity theory. While non-idealities certainly exist, Equations (4) and (7) enable the rational design of a polymeric viscoelastic material that could serve as a biophysical mimic for complex tissues.

Frequency sweeps of **4-H:4-AA** (Figure 2b) and **4-H:4-BA** (Figure SI 2b) indicate that the 32-fold difference in k_{-1} dramatically changes the ability of the materials to adapt to strain. **4-H:4-AA** exhibits a frequency-dependent modulus that is characteristic of a single-mode Maxwell viscoelastic fluid, whereas **4-H:4-BA** exhibits a frequency-independent modulus indicative of a Hookean solid. Presumably, the angular frequency at which G″ crosses G′ is lower than could be accurately

measured. Using Equations (4) and (5) for a Maxwellian viscoelastic fluid,[48]

$$G'(\omega) = \frac{G_\infty \omega^2 \tau^2}{1 + \omega^2 \tau^2}, \quad (4)$$

$$G''(\omega) = \frac{G_\infty \omega \tau}{1 + \omega^2 \tau^2} \quad (5)$$

where G_∞ is the equilibrium modulus, ω is the angular frequency, and τ is the relaxation time; we find τ = 34 s (Figure 2b). This agreement with the Maxwell model indicates that these gels should relax an applied stress on a time scale on the order of tens of seconds and that by varying the ratio of benzaldehyde to aliphatic aldehyde crosslinker, one should retain a great deal of control over the adaptation properties of the material.

Thus, we next polymerized six gels of varying compositions, ranging from 100% **4-AA** crosslinks to 100% **4-BA** crosslinks and strained them 100% on the rheometer (Figure 2c). Gels crosslinked by 100% aliphatic aldehyde macromers relaxed 100% of their stress within tens of seconds, while those crosslinked by 100% benzaldehyde macromers took closer to 14 hours to relax 75% of their stress, although it is likely there is some error associated with these measurements due to instrument slippage (Figure SI 3a). We observed that the stress relaxation profile can be adjusted by changing the ratio of aliphatic aldehyde to benzaldehyde macromer: as the proportion of benzaldehyde macromer increases, the hydrogel relaxes stress more slowly, until a critical point, the percolation threshold (vide infra), is reached (Figure 2c). Thus, by tuning these characteristics — the number of arms on the PEG polymer, the choice of either aliphatic aldehyde or benzaldehyde end groups, the ratio of the aliphatic to aryl aldehyde-derivatized macromers, and the relative stoichiometry of hydrazine and aldehyde components — it is possible to precisely control the physiological modulus and stress relaxation characteristics of the gel to tailor the gel characteristics specifically to the tissue under study.

Next, we fit the relaxation data to Equation (6), a standard Maxwell model for viscoelastic fluids,[49]

$$G(t) = \sum_{k=1}^{N} \frac{\eta k}{\lambda_k} e^{-\frac{t}{\lambda k}} + G_\infty \quad (6)$$

where G_∞ is the elastic modulus, η is the viscosity, and λ is the time constant of relaxation. While all adaptable gels should have a polymer relaxation mode and a bond relaxation mode, the rapid relaxation of the polymer chains (typical λ = 0.05 s) was not captured in the rheology. The 4-arm-co-4-arm (**4-H:4-AA**) aliphatic gel fit the model well with a single mode of relaxation (λ = 10.7 s), as did the 8-arm-co-8-arm (**8-H:8-AA**) aliphatic gel (λ = 91.0 s). These numbers are consistent with the fact that at equal weight percent of PEG, the 8-arm-co-8-arm gels contain 8-fold more crosslinks, leading to a roughly 8-fold slower time constant of relaxation. The benzaldehyde crosslinked gels did not fit the model as well, which is likely a result of slow relaxation competing with instrument slip. However, the **4-H:4-BA** gel relaxed with a time constant of λ = 2370 s, while the **8-H:8-BA** gel tore before 100% strain could be applied, which precluded accurate measurement of the time constant. Mixed crosslink gels containing a fraction of benzaldehyde crosslinkers below the percolation threshold, calculated using Equations (7) and (8),[50–52]

$$p_c = \frac{1}{\sqrt{\frac{(f_A - 1)(f_B - 1)}{r}}}, \quad (7)$$

$$r = \frac{f_B n_B}{f_A n_A} \quad (8)$$

which equals 0.33 for **4-H:4-AA** and **4-H:4-BA**, are modeled reasonably well in their early and late stages by summing both the aliphatic aldehyde and the benzaldehyde modes (Figure SI 4). However, once the gel is comprised of more than 33% **4-BA** crosslinks, the stress relaxation behavior of these materials collapses to that of **4-H:4-BA**. Finally, when the gel is treated with sodium cyanoborohydride, the hydrazone bond is reduced to the corresponding hydrazine, thus abolishing the dynamic nature of the bond and, consequently, the relaxation behavior (Figure 2c).

The self-healing, dynamic characteristics of **4-H:4AA** and static nature of **4-H:4-BA** were also visualized macroscopically. Figure 2d shows two disk-shaped hydrogels formed using a syringe mold 5 mm in diameter. Both hydrogels were then pressed into a 4 mm × 4 mm square mold for 60 s, re-imaged, pressed into a 6 mm × 7 mm right triangular mold for 60 s, and imaged again. These qualitative images clearly demonstrate that **4-H:4-AA** has the capacity to rearrange its macroscopic network structure to relax stresses applied by the mold within 60 s, allowing it to be re-processed into a new macroscopic shape. On the contrary, **4-H:4-BA** is immutable on this time scale and retains its original disk shape throughout the processing. Though the aryl hydrazone bonds can relax stress, albeit on a much longer time scale than the aliphatic hydrazone bonds, we observed no shape change, even after 1 hour. Figure SI 5 further explores these macroscopic demonstrations of stress relaxation and shows the fusion of three gels into a larger shape, their molding into other shapes, and finally their injection through an 18 G needle to form a long extruded fiber.

We next sought to directly compare the viscoelastic properties of these hydrogel networks to that of a complex tissue, namely a mouse gastrocnemius muscle. We selected muscle for comparison, as it is widely known to relax stress in two separate modes, with a fast λ varying from 0.03 s to 8.4 s and a slow λ varying from 2.2 s to 93.8 s, depending on the species.[53] Further, muscle has a Young's modulus around 10 kPa, which is well within the range of the moduli for the PEG networks that were synthesized here (1.8 – 27 kPa).[18,53–55] A mouse gastrocnemius muscle was isolated and characterized using shear rheology. The results show a highly frequency-dependent elastic modulus between 2–3 kPa and relaxation of 80% of an applied stress within 600 seconds (**Figure 3**a, 3b). Consistent with mechanical theories of fiber containing composite materials,[56] we hypothesized that the steep reduction in modulus below 1 rad/s shear was due primarily to the fibrous structure of skeletal muscle, rather than formation and reformation of physical crosslinks. Interestingly, the stress relaxing hydrogels capture

Adv. Mater. 2013,
DOI: 10.1002/adma.201303680

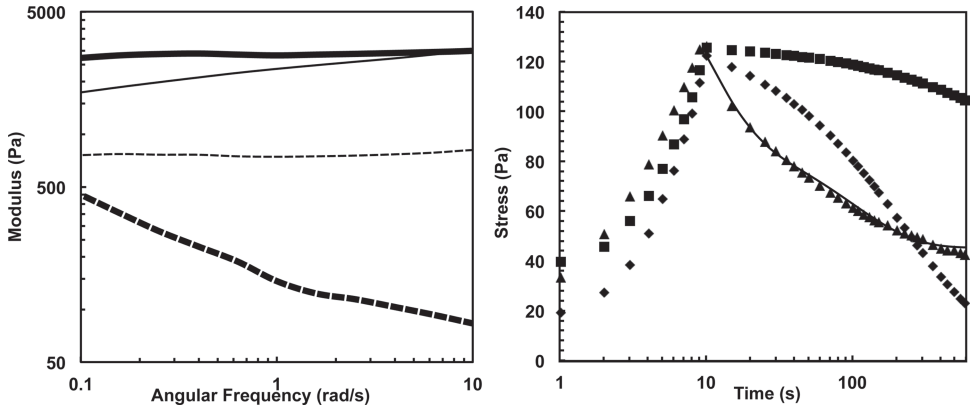

Figure 3. The rheological properties of complex tissue can be emulated using covalently adaptable hydrogels. a) The elastic modulus of mouse muscle (thin solid line, G′; thin dashed line, G″) begins to sharply decrease below 1 rad/s, possibly due to the fibrous nature of the tissue, while the **8-H:8-AA** (thick solid line, G′; thick dashed line, G″) exhibits this property below 0.05 rad/s. However, G_∞ of the mouse muscle can be exactly matched. b) The mouse muscle (triangles) demonstrates significant stress relaxation over 10 minutes and fits a two-mode Maxwell model (solid line). **8-H:8-AA** (diamonds) comes close to reproducing the initial and final stress with just one mode of relaxation. **8-H:8-BA** (squares) relaxes much more slowly.

aspects of this behavior through breaking and reforming of the material crosslinks, and we observed two discrete modes of relaxation and fit them to a two-mode Maxwell model.[53,54,57] This behavior is readily seen in Figure 3b, where the applied stress initially decays rapidly and then slows. In contrast, the trace of the 100% **8-H:8-AA** gel displays a single mode of relaxation. When fit to the Maxwell model, muscle relaxes with time constants of $\lambda = 7.5$ s and $\lambda = 100$ s with a ca. 55% weighting of the slow-relaxing mode and a ca. 45% weighting of the fast-relaxing mode. These values are consistent with published measurements of tensile muscle relaxation,[53,54] and they fall within the range of the relaxation time constants of the 4-arm ($\lambda = 10.7$ s) and 8-arm aliphatic gels ($\lambda = 91.0$ s). Collectively, these results suggest that covalently adaptable networks impart unique viscoelastic properties that mimic aspects of native tissue materials that are difficult to capture with traditional synthetic hydrogels. Further, by tuning the initial macromer composition and concentration (**8-H:8-AA, 2:1 ratio)**, gels were formulated with initial and time dependent properties very similar to those of the gastrocnemius.

We next sought to demonstrate the cytocompatibility of the reaction and encapsulation processes and examine how cells would respond to longer-term culture in these covalently adaptable networks. Because of our characterization of mouse skeletal muscle, this compelled us to examine a cell line, C2C12s, a common source of myoblasts that fuse into myotubes under confluent conditions. For cell encapsulation studies, we formulated three hydrogels using the hydrazine- and aldehyde-terminated PEG macromers in combination with a benzaldehyde-terminated KGRGDS peptide, which provides sites for integrin binding and promotes cell survival in PEG gels.[58–61] Specifically, one gel was synthesized with 100% aliphatic crosslinks (**8-H:8-AA**), another with 80% aliphatic crosslinks and 20% aryl aldehyde crosslinks (**8-H:(80% 8-AA 20% 8-BA)**), and a final gel with 100% aryl aldehyde crosslinks (**8-H:8-BA**). All gels contained 3 mM KGRGDS peptide. We selected these specific compositions to form highly adaptable gels that would remain stable for several weeks of cell culture (Figure SI 3b) yet allow a significant variation in stress relaxation properties, from highly relaxing to minimally relaxing. C2C12 myoblasts were encapsulated at a concentration of 10^6 cells/mL, and the cells were stained and imaged for viability after 24, 72, and 240 hours (**Figure 4**a, 4b, Figure SI 6) and cytoskeletal organization at 24, 96, 144, and 264 hours (Figure 4c, Figure SI 7).

First, we note high levels of cell survival after encapsulation, thus validating the applicability of this crosslinking chemistry for the conditions studied (Figure 4a, 4b). Calcein-AM and ethidium homodimer staining indicated that viability was higher than 90% in all three conditions after 72 h (Figure 4b), which confirms that this hydrogel platform is cytocompatible and appropriate for studying cellular responses to dynamic, tissue-mimicking biophysical environments. Furthermore, the significant drop in cell viability in **8-H:8-BA** after 10 days in culture implies that matrix dynamism could play an important role in long-term cell viability (Figure 4b). Cells maintain a rounded morphology when encapsulated in covalently crosslinked hydrogels, so we next sought to examine how cells would behave in hydrogels in which the crosslinks dynamically break and re-form.[10,14] Interestingly, we observed that after only 24 hours in culture, a minority of the cells encapsulated in the **8-H:8-AA** gels extended small filopodia and lamellipodia, while those in the **8-H:(80% 8-AA 20% 8-BA)** and **8-H:8-BA** gels retained their circular morphology. By 72 hours, however, nearly all cells in the **8-H:8-AA** gels began to extend processes, while those in the **8-H:8-BA** gels remained rounded; the **8-H:(80% 8-AA 20% 8-BA)** gels contained cells of both phenotypes (Figure SI 6). At later time points, the filopodia and lamellipodia became more pronounced, and essentially all cells in both the **8-H:8-AA** and **8-H:(80% 8-AA 20% 8-BA)** gels had begun to spread. By 10 days in culture, the cells in the **8-H:8-AA** gels demonstrated the spread myoblast phenotype (Figure 4c, Figure SI 7), and some cells with close neighbors began to fuse into multinucleated structures demonstrating a myotube-like morphology with continuous actin filaments spanning the entire mass (Figure 4d). This myoblast fusion suggests the beginning

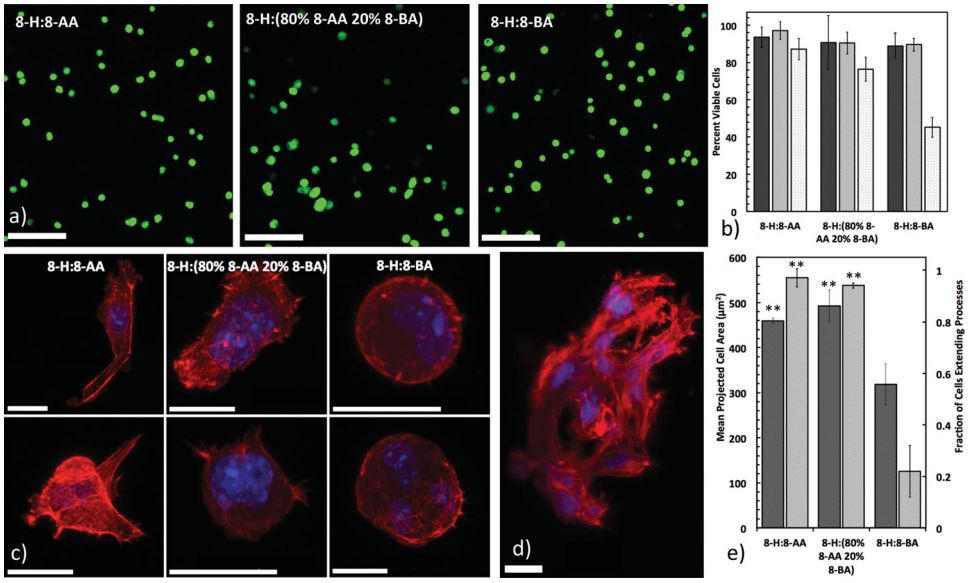

Figure 4. a) Images of encapsulated C2C12 myoblasts 72 hours post-encapsulation stained with calcium-AM (green, live) and ethidium homodimer (red, dead; scale bar 200 μm). b) Cell viability quantified at 24 hours (dark bars), 72 hours (medium bars), and 240 hours (light bars). c) Representative images of cells stained for f-actin (red) and the nucleus (blue) are shown (scale bar 20 μm). After 10 days in culture, the cells encapsulated in **8-H:8-AA** exhibit significant spreading and robust actin fiber formation. Cells encapsulated in **8-H:(80% 8-AA,20% 8-BA)** extend lamellipodia and filopodia and show actin filaments but do not deviate as far from rounded. Cells encapsulated in **8-H:8-BA** remain rounded. d) Some cells in the **8-H:8-AA** gels fuse into multinuclear structures. e) Quantification of cell spreading (dark bars, left axis) and fraction of cells extending processes (light bars, right axis) by 10 days in culture. Cells in **8-H:8-AA** and **8-H:(80% 8-AA,20% 8-BA)** both displayed significantly more spreading, as measured by projected cell area and process extension, than those in **8-H:8-BA** (Student's t-test, $p<0.05$).

stages of differentiation; this process did not happen to cells in **8-H:8-BA**. C2C12s in **8-H:(80% 8-AA 20% 8-BA)** displayed significant process extension, but while their mean projected cell area was not significantly different from the cells in **8-H:8-AA**, they retained a more rounded morphology. Furthermore, we observed fewer fused multinuclear structures. Cells in the less-dynamic **8-H:8-BA** gels remained rounded, even after 10 days with less than 30% of cells extending processes into the material (Figure 4c). These results were quantified by measuring the mean projected cell area and counting the number of cells extending processes into the material. We found that cells in **8-H:8-AA** and **8-H:(80% 8-AA 20% 8-BA)** both displayed significantly higher mean cell projected areas and a higher fraction of cells extending processes than cells in **8-H:8-BA** (Figure 4e). Based on these three-dimensional observations, we propose that the dynamic nature of the aliphatic hydrazone linked hydrogel allows the gel to rearrange on a timescale that is compatible with filopodia and lamellipodia extension, and thus, the material can accommodate cytoskeletal outgrowth. In contrast, the more slowly relaxing gels, such as **8-H:8-BA**, produce a much more static matrix that constrains the cells to a circular morphology throughout the course of the experiment. Rheological experiments on cell-laden gels show that the incorporation of cells lowers the equilibrium modulus but does not significantly change the stress relaxation properties (Figure SI 8a and 8b). SEM imaging reveals that the hydrogels are amorphous solids lacking pores or ordered structure (Figure SI 9). Given the constancy of the stress relaxing properties and the lack of pores or order, it is likely that encapsulated cells apply stress, which leads to a dynamic rearrangement of the hydrazone bonds and allows them to spread out in the material.

Here, we examined the simulation of muscle and encapsulation of myoblasts, but this cytocompatible covalently adaptable hydrogel could be applied to other cellular systems where viscoelasticity or careful control of the scaffold biophysical properties is desirable. For instance, it is known that reduced crosslinking in the pericellular environment induces increased proliferation in myofibroblasts,[15] and this covalently adaptable hydrogel could be used to quantify the degree of stress necessary to inhibit proliferation and the kinetics of the associated signaling pathways. Scaffold mechanics and cell shape have both been implicated in progenitor cell differentiation,[18,62,63] but decoupling these two phenomena is challenging in cell degradable gels. Covalently adaptable gels allow the study of progenitor cells in a defined biophysical environment while simultaneously allowing cells to adopt their preferred geometries. Finally traditional covalent gels force secreted ECM molecules into a confined geometry,[5] preluding the assembly of micron-size features like collagen fibers. Covalently adaptable networks may prove a useful system to respond and accommodate the assembly of secreted ECM and subsequent collagen fiber formation.

We have developed a cytocompatible covalent adaptable hydrogel capable of mimicking the modulus and stress relaxation properties of many complex biological tissues. Here, we have described a material that simulates some of the properties of native mouse muscle and demonstrated its utility as a

Adv. Mater. **2013**,
DOI: 10.1002/adma.201303680

scaffold to culture mouse myoblasts. The modular nature of hydrogel construction and the large number of easily tuned variables provide access to gels with a wide range of modulus and stress relaxation characteristics; the same approach could potentially be applied to nearly any tissue in the body. C2C12 cell encapsulation studies demonstrate that these covalently adaptable hydrogels allow for the development of physiologically relevant morphologies, whereas static, non-adaptable gels prevent cytoskeletal rearrangement and extension. Taken together, these studies show that hydrazone linked hydrogels offer unique advantages in terms of dynamic tunability and should serve as a valuable complement to existing hydrogel technologies.

Supporting Information

Supporting Information is available from the Wiley Online Library or from the author.

Acknowledgements

The authors acknowledge Martin Guess in Prof. Leslie Leinwand's lab for the generous gift of the C2C12 cells and the mouse gastrocnemius muscle, Drs. Malar Azagarsamy and Daniel Alge for helpful discussions related to chemistry and material properties, and Dr. Kelly Schultz for her invaluable input regarding rheological characterization. These studies were supported by a grant from the NSF (DMR 1006711), the NIH Pharmaceutical Biotechnology Training Program (5 T32 GM 8732), Office of Naval Research (N00014–13–1–0283), and the Howard Hughes Medical Institute.

Received: August 7, 2013
Revised: August 23, 2013
Published online:

[1] B. V. Slaughter, S. S. Khurshid, O. Z. Fisher, A. Khademhosseini, N. A. Peppas, *Adv. Mater.* **2009**, *21*, 3307–3329.
[2] J. L. Drury, D. J. Mooney, *Biomaterials* **2003**, *24*, 4337–4351.
[3] O. Guillame-Gentil, O. Semenov, A. S. Roca, T. Groth, R. Zahn, J. Vörös, M. Zenobi-Wong, *Adv. Mater.* **2010**, *22*, 5443–5462.
[4] S. J. Bryant, K. S. Anseth, *J. Biomed. Mater. Res.* **2001**, *59*, 63–72.
[5] S. J. Bryant, K. S. Anseth, *J. Biomed. Mater. Res.* **2002**, *64A*, 70–79.
[6] S. J. Bryant, K. L. Durand, K. S. Anseth, *J. Biomed. Mater. Res.* **2003**, *67A*, 1430–1436.
[7] M. P. Lutolf, J. A. Hubbell, *Biomacromolecules* **2003**, *4*, 713–722.
[8] B. D. Fairbanks, M. P. Schwartz, A. E. Halevi, C. R. Nuttelman, C. N. Bowman, K. S. Anseth, *Adv. Mater.* **2009**, *21*, 5005–5010.
[9] J. Benton, B. Fairbanks, K. S. Anseth, *Biomaterials* **2009**, *30*, 6593–6603.
[10] S. B. Anderson, C. C. Lin, D. V. Kuntzler, K. S. Anseth, *Biomaterials* **2011**, 3564–3574.
[11] K. A. Kyburz, K. S. Anseth, *Acta Biomater.* **2013**, DOI 10.1016/j.actbio.2013.01.026.
[12] M. P. Schwartz, B. D. Fairbanks, R. E. Rogers, R. Rangarajan, M. H. Zaman, K. S. Anseth, *Integr. Biol.* **2010**.
[13] J. Shepard, A. Stevans, S. Holland, C. E. Wang, A. Shikanov, L. D. Shea, *Biotechnol. Bioeng.* **2012**, *109*, 830–839.
[14] D. D. McKinnon, A. M. Kloxin, K. S. Anseth, *Biomaterials Science* **2013**, *1*, 460–469.
[15] J. Patterson, J. A. Hubbell, *Biomaterials* **2010**, *31*, 7836–7845.
[16] T. P. Kraehenbuehl, P. Zammaretti, A. J. van der Vlies, R. G. Schoenmakers, M. P. Lutolf, M. E. Jaconi, J. A. Hubbell, *Biomaterials* **2008**, *29*, 2757–2766.
[17] S. T. Lee, J. I. Yun, Y. S. Jo, M. Mochizuki, A. J. van der Vlies, S. Kontos, J. E. Ihm, J. M. Lim, J. A. Hubbell, *Biomaterials* **2010**, *31*, 1219–1226.
[18] A. Engler, S. Sen, H. Sweeney, D. E. Discher, *Cell* **2006**, *126*, 677–689.
[19] A. M. Kloxin, J. A. Benton, K. S. Anseth, *Biomaterials* **2010**, *31*, 1–8.
[20] J. Zoldan, E. D. Karagiannis, C. Y. Lee, D. G. Anderson, R. Langer, S. Levenberg, *Biomaterials* **2011**, *32*, 9612–9621.
[21] M. Guvendiren, J. A. Burdick, *Nat. Commun.* **2012**, *3*, 792.
[22] L. Weng, A. Romanov, J. Rooney, W. Chen, *Biomaterials* **2008**, *29*, 3905–3913.
[23] L. Weng, X. Chen, W. Chen, *Biomacromolecules* **2007**, *8*, 1109–1115.
[24] H. Zhang, A. Qadeer, W. Chen, *Biomacromolecules* **2011**, *12*, 1428–1437.
[25] S. K. Bhatia, S. D. Arthur, H. K. Chenault, G. K. Kodokian, *Biotechnol. Lett.* **2007**, *29*, 1645–1649.
[26] J. Dahlmann, A. Krause, L. Möller, G. Kensah, M. Möwes, A. Diekmann, U. Martin, A. Kirschning, I. Gruh, G. Dräger, *Biomaterials* **2013**, *34*, 940–951.
[27] X. Chen, M. A. Dam, K. Ono, A. Mal, H. Shen, S. R. Nutt, K. Sheran, F. Wudl, *Science* **2002**, *295*, 1698–1702.
[28] C. N. Bowman, C. J. Kloxin, *Angew. Chem. Int. Ed.* **2012**, 4272–4274.
[29] G. Deng, C. Tang, F. Li, H. Jiang, Y. Chen, *Macromolecules* **2010**, *43*, 1191–1194.
[30] C. J. Kloxin, T. F. Scott, B. J. Adzima, C. N. Bowman, *Macromolecules* **2010**, *43*, 2643–2653.
[31] B. J. Adzima, C. J. Kloxin, C. N. Bowman, *Adv. Mater.* **2010**, *22*, 2784–2787.
[32] T. F. Scott, A. D. Schneider, W. D. Cook, C. N. Bowman, *Science* **2005**, *308*, 1615–1617.
[33] C. J. Kloxin, T. F. Scott, H. Y. Park, C. N. Bowman, *Adv. Mater.* **2011**, *23*, 1977–1981.
[34] M. C. Roberts, M. C. Hanson, A. P. Massey, E. A. Karren, P. F. Kiser, *Adv. Mater.* **2007**, *19*, 2503–2507.
[35] S. J. Rowan, S. J. Cantrill, G. R. L. Cousins, J. K. M. Sanders, J. F. Stoddart, *Angew. Chem. Int. Ed.* **2002**, *41*, 898–952.
[36] V. T. Bhat, A. M. Caniard, T. Luksch, R. Brenk, D. J. Campopiano, M. F. Greaney, *Nat. Chem.* **2010**, *2*, 490–497.
[37] G. Iyer, F. Pinaud, J. Xu, Y. Ebenstein, J. Li, J. Chang, D. Maxime, S. Weiss, *Bioconjugate Chem.* **2011**, *22*, 1006–1011.
[38] A. Dirksen, S. Dirksen, T. M. Hackeng, P. E. Dawson, *J. Am. Chem. Soc.* **2006**, *128*, 15602–15603.
[39] A. Dirksen, S. Yegneswaran, P. E. Dawson, *Angew. Chem. Int. Ed.* **2010**, *49*, 2023–2027.
[40] A. Dirksen, P. E. Dawson, *Bioconjugate Chem.* **2008**, *19*, 2543–2548.
[41] A. R. Blanden, K. Mukherjee, O. Dilek, M. Loew, S. L. Bane, *Bioconjugate Chem.* **2011**, *22*, 1954–1961.
[42] J. Kalia, R. T. Raines, *Angew. Chem. Int. Ed.* **2008**, *47*, 7523–7526.
[43] D. W. Domaille, J. H. Lee, J. N. Cha, *Chem. Commun.* **2013**, *49*, 1759–1761.
[44] M. Karver, R. Weissleder, *Angew. Chem. Int. Ed.* **2012**, *51*, 920–922.
[45] J. W. Bae, E. Lee, K. M. Park, K. D. Park, *Macromolecules* **2009**.
[46] J. Xu, T. M. Filion, F. Prifti, J. Song, *Chem. Asian J.* **2011**, *6*, 2730–2737.
[47] J. Zheng, L. A. Smith Callahan, J. Hao, K. Guo, C. Wesdemiotis, R. A. Weiss, M. L. Becker, *ACS Macro Lett.* **2012**, *1*, 1071–1073.
[48] T. Annable, *J. Rheol.* **1993**, *37*, 695–726.
[49] F. A. Morrison, *Understanding Rheology*, Oxford University Press, USA **2001**.
[50] P. J. Flory, *J. Am. Chem. Soc.* **1941**, *63*, 3083–3090.
[51] P. J. Flory, *J. Phys. Chem.* **1942**, *46*, 132–140.

[52] W. H. Stockmayer, *J. Chem. Phys.* **1943**, *11*, 45.
[53] B. C. Abbott, J. Lowy, *Proc. R. Soc. B* **1957**, *146*, 281–288.
[54] A. Magid, D. J. Law, *Science* **1985**.
[55] A. J. Engler, M. A. Griffin, S. Sen, C. G. Bönnemann, H. L. Sweeney, D. E. Discher, *J. Cell Biol.* **2004**, *166*, 877–887.
[56] S. Onogi, K. Ui, *Journal of Colloid Science* **1956**, *11*, 214–225.
[57] K. W. Ranatunga, *J. Muscle Res. Cell Motil.* **2001**, *22*, 399–414.
[58] M. D. Pierschbacher, E. Ruoslahti, *Nature* **1984**, *309*, 30–33.
[59] J. A. Burdick, K. S. Anseth, *Biomaterials* **2002**, *23*, 4315–4323.
[60] C. R. Nuttelman, M. C. Tripodi, K. S. Anseth, *Matrix Biol.* **2005**, *24*, 208–218.
[61] E. A. Phelps, N. O. Enemchukwu, V. F. Fiore, J. C. Sy, N. Murthy, T. A. Sulchek, T. H. Barker, A. J. García, *Adv. Mater.* **2011**, *24*, 64–70.
[62] R. McBeath, D. M. Pirone, C. M. Nelson, K. Bhadriraju, C. S. Chen, *Dev. Cell* **2004**, *6*, 483–495.
[63] K. A. Kilian, B. Bugarija, B. T. Lahn, M. Mrksich, *Proc. Natl. Acad. of Sci.* **2010**, *107*, 4872–4877.

Adv. Mater. **2013**,
DOI: 10.1002/adma.201303680